Physics Letters B 770 (2017) 77–82

Contents lists available at ScienceDirect

Physics Letters B

www.elsevier.com/locate/physletb

Identification of the one-quadrupole phonon $2^+_{1,ms}$ state of ^{204}Hg

R. Stegmann [a,*], C. Stahl [a], G. Rainovski [b], N. Pietralla [a], C. Stoyanov [c], M.P. Carpenter [d], R.V.F. Janssens [d], M. Lettmann [a], T. Möller [a], O. Möller [a], V. Werner [a], S. Zhu [d]

[a] Institut für Kernphysik, Technische Universität Darmstadt, Darmstadt, Germany
[b] Faculty of Physics, University of Sofia St. Kliment Ohridski, Sofia, Bulgaria
[c] Institute for Nuclear Research and Nuclear Energy, Bulgarian Academy of Sciences, Sofia, Bulgaria
[d] Physics Division, Argonne National Laboratory, Argonne, USA

ARTICLE INFO

Article history:
Received 17 January 2017
Received in revised form 5 April 2017
Accepted 6 April 2017
Available online 19 April 2017
Editor: V. Metag

Keywords:
γ ray spectroscopy
Coulomb excitation
Quadrupole collectivity
Isospin degree of freedom
Shell structure

ABSTRACT

One-phonon states of vibrational nuclei with mixed proton–neutron symmetry have been observed throughout the nuclear chart besides the mass $A \approx 200$ region. Very recently, it has been proposed that the 2^+_2 state of ^{212}Po is of isovector nature. This nucleus has two valence protons and two valence neutrons outside the doubly-magic ^{208}Pb nucleus. The stable isotope ^{204}Hg, featuring two valence-proton and valence-neutron holes, with respect to ^{208}Pb, is the particle-hole mirror of ^{212}Po. In order to compare the properties of low-lying isovector excitations in these particle-hole mirror nuclei, we have studied ^{204}Hg by using the projectile Coulomb-excitation technique. The measured absolute $B(M1; 2^+_2 \rightarrow 2^+_1)$ strength of $0.20\,(2)\,\mu^2_N$ indicates that the 2^+_2 level of ^{204}Hg is at least the main fragment of the $2^+_{1,ms}$ state. For the first time in this mass region, both lowest-lying, one-quadrupole phonon excitations are established together with the complete set of their decay strengths. This allows for a microscopic description of their structures, achieved in the framework of the Quasi-particle Phonon Model.

1. Introduction

How collectivity emerges in many-body quantum systems is one of the fundamental issues in contemporary nuclear structure physics [1]. The proton–neutron interaction plays a crucial role in this process [2]. The properties of collective states in which valence protons and neutrons move out of phase contain sensitive information about the isovector part of the proton–neutron interaction. These isovector, valence-shell excitations are dubbed states with mixed proton–neutron symmetry [3,4]. Mixed-symmetry states (MSSs) appear naturally in the framework of the Interacting Boson Model-2 (IBM-2) [3,5] which distinguishes between proton and neutron bosons, alongside so-called fully-symmetric states (FSSs), where protons and neutrons are formally interchangeable. This is formalized by the so-called F spin quantum number which is the isospin analog for bosons [5]. For FSSs, the F spin is fully aligned ($F = F_{max}$), resulting in the nuclear wavefunction remaining unchanged with respect to the pairwise exchange of proton and neutron boson labels. For states where the F spin is not fully aligned ($F < F_{max}$), *i.e.*, MSSs, the wavefunction becomes sensitive to the exchange of proton and neutron bosons and, hence, to the effective proton–neutron interaction in the valence shell [6].

In vibrational nuclei, the lowest isovector valence-shell excitation is the one-phonon $2^+_{1,ms}$ state [4,5]. Due to its isovector character, it decays rapidly with a strong M1 transition to the one-phonon FSS, which is the 2^+_1 state of the nucleus being studied, as well as with a weakly-collective E2 transition to the ground state [7–11]. Since M1 transitions between states of the same F spin are forbidden [5], this unique decay serves as an unambiguous experimental signature for identification of one-phonon MSSs. In addition, due to the isovector character of the E1 operator [12], enhanced E1 transitions can be expected between fully symmetric octupole states and the MSSs of quadrupole character. These enhanced E1 transitions can serve as an additional signature for the identification of MSSs [13].

In weakly-collective, vibrational nuclei distinct examples of one-phonon MSSs have been found in stable nuclei of the mass $A \approx 90$ region [8,14,15]. Several examples of MSSs have been identified in the mass $A \approx 130$ region [6,16–20], as well. In the vicinity of the doubly-magic ^{208}Pb, so far only a single low-lying isovector state has been recently identified in $^{212}_{84}$Po [21]. The structure of the low-lying excitations of ^{212}Po is dominated by the $\pi\,(1h_{9/2})^2\,\nu(2g_{9/2})^2$ configuration. The experimental informa-

* Corresponding author.
E-mail address: rstegmann@ikp.tu-darmstadt.de (R. Stegmann).

http://dx.doi.org/10.1016/j.physletb.2017.04.032

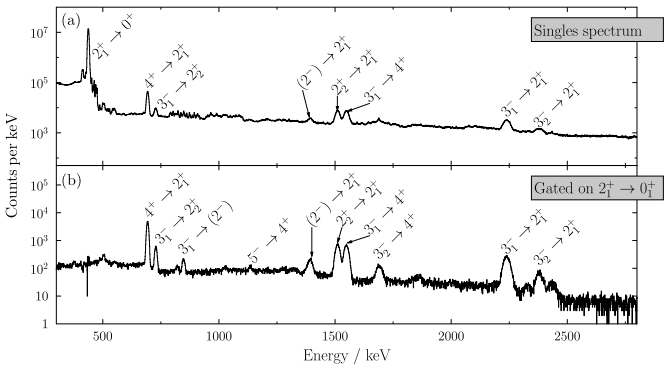

Fig. 1. Doppler-corrected, background-subtracted γ ray spectra after projectile Coulomb excitation on a ^{12}C target. In (a) the singles spectrum is shown; (b) provides the spectrum of γ rays in coincidence with the $2_1^+ \to 0_1^+$ transition. In both spectra the transitions relevant for this study are highlighted. The spectra are not corrected for efficiency.

tion accumulated up to now suggests that pronounced one-phonon MSSs can be expected when both protons and neutrons occupy orbitals with high angular momenta like in the case of ^{212}Po. The stable isotope ^{204}Hg, with a $\pi(2d_{3/2})^{-2}\,\nu(2f_{5/2})^{-2}$ valence structure with respect to ^{208}Pb, is the particle-hole mirror of ^{212}Po. Its structure is expected to be dominated by orbitals with smaller angular momenta for the valence-proton and valence-neutron holes as compared to ^{212}Po. It is interesting to investigate how the one-phonon MSS is formed in this valence space and to compare its properties in relation to those of the one-phonon MSS of ^{212}Po. In order to address this question, an experiment to search for the one-phonon MSS, $2^+_{1,ms}$, of ^{204}Hg was carried out.

2. Experiment

In the reported experiment, a ^{204}Hg beam was accelerated to 890 MeV by the ATLAS facility at Argonne National Laboratory. The pulsed beam (12 MHz) was guided on the target surrounded by the Gammasphere detector array [22], consisting of 100 HPGe detectors grouped in 16 rings. The spectrometer was operated in singles mode as the only condition for recording data was that at least any one HPGe detector detected a γ ray. The beam was impinging alternatively on 1 mg/cm^2-thick ^{12}C or 1 mm-thick Al targets. The ^{12}C target was used for the Coulomb excitation measurement, while the thick Al one was employed for level lifetime measurements by the Doppler Shift Attenuation Method (DSAM). The beam energy corresponds to $\approx 84\%$ of the Coulomb barrier for the ^{204}Hg + ^{12}C system. A total of 4.4×10^8 events of γ ray fold ≥ 1 was collected over a period of 13 h beam on the ^{12}C target. Spectra were corrected for the Doppler shift, adopting a projectile velocity of $v/c \approx 8.4\%$. The contribution of the room background was subtracted by correlating the γ rays with the accelerator radio-frequency (rf) signal. The final spectrum, which is a difference between the "beam-on" (with respect to the rf) and "beam-off" spectra, scaled to eliminate the 1461-keV room background ^{40}K transition, is given in Fig. 1(a).

This spectrum is dominated by the 437-keV, $2_1^+ \to 0^+$, transition of ^{204}Hg with 9.5×10^7 counts. All other strong γ rays originate from ^{204}Hg excited states [23–38] as well and most of these are in coincidence with the ground-state transition (cf. Fig. 1(b)). Besides ^{204}Hg transitions, the spectrum in Fig. 1(a) also contains numerous weak transitions of narrow widths that originate from fusion-evaporation reactions caused by target-like nuclei scattered on materials of the target chamber and the beam pipe. Although present in the spectrum, these γ rays from stopped sources are smeared out by the Doppler correction for the mean velocity of excited beam ions and, hence, only contribute to an increase in the background which results in larger statistical uncertainties in specific cases.

The level scheme, including the levels of ^{204}Hg populated in the present Coulomb excitation experiment, is shown in Fig. 2. There are a few candidates for spin-2 states. The next-to-lowest of these is the level at 1829 keV, for which, however, a negative parity is favored [39]. This level decays exclusively to the 2_1^+ state via a 1392-keV transition. The next level of this group is located at 1851 keV, has a demonstrated positive parity, but its spin value is suggested to be either 2 or 3 [39]. This level decays predominantly to the 4_1^+ state via the 723-keV transition. The decay to the 2_1^+ level was not observed, but the branching ratio is known [23]. In this respect, the present experiment does not provide any new information which could determine more firmly the spin and/or parity quantum numbers of these two levels. It has to be noted that a known state at 1716 keV with a tentative spin-parity assignment (2^+) [25,26] is not populated in this experiment – the 1280-keV γ ray is not present in either the singles spectrum or in the coincidence data gated on the 437-keV transition (see Fig. 1).

Additional 2^+ levels at 1948 and 1989 keV were populated as well. Several measurements favor 2^+ assignments for these two levels [39]. Both of them decay predominantly to the 2_1^+ state. While the transition from the 1948-keV level to the ground state could not be observed, its intensity was determined via the known branching ratio $I_{\gamma,2_2^+\to 0^+}/I_{\gamma,2_2^+\to 2_1^+} = 5.3\,(4)\,\%$ [23]. The level at 1989 keV decays to the ground state and to the 2_1^+ level. The data include no additional transitions to the ground state. The observed decay patterns for the 1948- and 1989-keV levels unambiguously fix their spin-parities to 2^+ and, since these are the only off-yrast 2^+ levels with fixed spin-parity assignments, we have labeled them as 2_2^+ and 2_3^+, respectively.

Two 3^- states, at 2675 and 2813 keV, and a 5^- level at 2263 keV are observed as well. The data obtained with the thick Al target yield consistent results. In that part of the measurement all projectile nuclei were stopped in the thick Al target. In the corresponding spectra, some γ rays from strongly populated states exhibit significant Doppler shapes, indicating sensitivity to the respective lifetimes (see below).

3. Analysis and results

The ansatz of combining information from the DSAM lifetime measurement and the projectile Coulomb excitation ultimately results in the possibility of identifying the $2^+_{1,ms}$ state of ^{204}Hg.

3.1. Coulomb excitation analysis

The intensities of the observed γ rays, from the known branching ratios and the theoretical electron-conversion coefficients [40], determine the Coulomb excitation (CE) yields for the populated levels of ^{204}Hg. The yields, relative to that of the 2_1^+ state, measure the relative CE cross sections. These data were fitted to the Winther–de Boer theory [41] using the multiple CE code CLX [42] while taking into account the energy loss of the beam in the target. Absolute cross sections were derived using the previously measured value for the transition probability $B(E2; 2_1^+ \to 0^+) = 11.96\,(9)$ W.u. [24,32,39,43], and the known quadrupole moment of the 2_1^+ state [32]. In the analysis, the quadrupole moment of the 2_2^+ level was varied within the limits of the quadrupole moment of the fully-symmetric 2_1^+ state from $0.20 - 0.60$ eb, which introduces an additional uncertainty for the matrix elements of about 1 %.

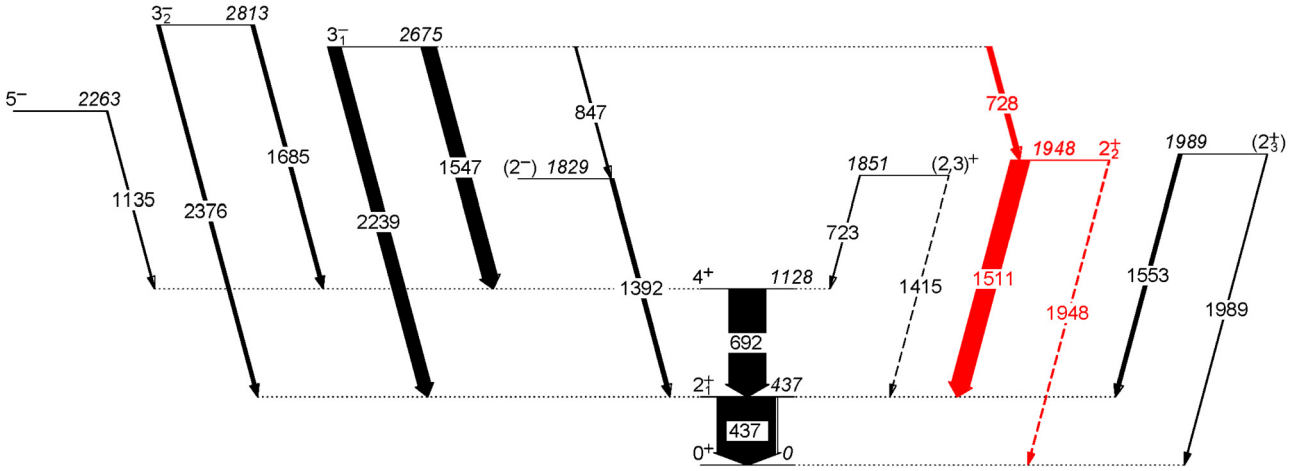

Fig. 2. (Color online.) Experimental level scheme of ^{204}Hg from this work. The thickness of the arrows corresponds to the intensity determined from experimental data. The $2_1^+ \rightarrow 0^+$ transition intensity is scaled down to fit into this image. Transitions connected to the 2_2^+ level are highlighted as this state is the candidate for the $2^+_{1,ms}$ MSS. The dashed transitions were not observed in this experiment, but the branching ratios have been measured in earlier work [23].

Table 1
Measured properties of the levels and γ ray transitions in ^{204}Hg in standard notation. The γ ray intensities are corrected for relative efficiencies and scaled down to improve readability.

E_{Level} (keV)	J^π	E_γ (keV)	J_f^π	I_γ	A_2/A_0	A_4/A_0	δ	τ[a] (fs)	$\pi\lambda$	$B(\pi\lambda)\downarrow$[b,c]	$B(\pi\lambda)_{\text{lit}}$[c,d]
437	2_1^+	437	0^+	$1.73(2)\cdot 10^6$	0.000(12)	0.006(18)			E2		11.96(9) [39]
1128	4_1^+	692	2_1^+	935(13)	0.119(16)	−0.006(23)	E2[e]		E2	14.9(47)	17.0(13) [31]
		1128	0^+						E4		5.5(7) [24]
1829	(2^-)	1392	2_1^+	97(2)	0.218(53)	0.088(72)					
1851	$(2,3)^+$	723	4_1^+	15(2)							
		1415	2_1^+	5.8(8)[g]							
1948	2_2^+	1511	2_1^+	461(9)	0.319(27)	−0.025(38)	0.260(81)	$84.6^{+14.2}_{-7.4}$	M1	0.200(23)	
									E2	1.19(71)	
		1948	0^+	24(2)[g]					E2	0.280(21)	
1989	2_3^+	1553	2_1^+	88(6)			E2 [25]		E2	1.55(38)	
		1989	0^+	20(2)					E2	0.099(24)	
2263	5^-	1135	4_1^+	29(2)							
2675	3_1^-	728	2_2^+	111(3)				232(30)	E1	0.413(56)	
		847	(2^-)	38(2)					E2	5.10(72)	
		1547	4_1^+	375(11)	0.072(26)	−0.006(37)			E1	0.145(19)	
		2239	2_1^+	324(15)	−0.091(36)	0.015(54)			E1	0.0412(56)	
		2675	0^+	< 1.1					E3	20.5(17)	23(2) [39]
2813	3_2^-	1685	4_1^+	85(4)							
		2376	2_1^+	80(4)							
		2813	0^+	< 9.3					E3	5.14(40)	8.03(92) [24]

[a] Extracted via DSAM analysis.
[b] Extracted via Coulomb-excitation analysis in the present experiment.
[c] $B(M1)$ values are given in $\mu_N{}^2$, $B(E1)$ values are given in mW.u., $B(E2)$, $B(E3)$ and $B(E4)$ values are given in W.u. (1 W.u. (E1) = $2.23\,e^2\,fm^2$, 1 W.u. (E2) = $71.3\,e^2\,fm^4$, 1 W.u. (E3) = $2.47\times10^3\,e^2\,fm^6$, 1 W.u. (E4) = $9.06\times10^4\,e^2\,fm^8$).
[d] The values in this column are the ones given within [39], converted to single-particle units.
[e] Treated as a pure-E2 transition. The angular distribution is washed out because of deorientation effects.
[g] Calculated via literature branching ratios.

The high detection efficiency of Gammasphere permits measurements of angular distributions for sufficiently intense transitions, allowing to extract the A_2/A_0 and A_4/A_0 coefficients given in Table 1. The $3_1^- \rightarrow 2_1^+$ transition at 2239 keV serves as a benchmark for this method, exhibiting a clear dipole character with vanishing A_4 and negative A_2 coefficients. The angular distribution of the $4_1^+ \rightarrow 2_1^+$ transition is not clearly observed, most likely due to the relatively long lifetime (4.2 (3) ps [31]) of the 4_1^+ state which may lead to a substantial attenuation of the anisotropy when excited ^{204}Hg nuclei recoil in vacuum [44]. This effect is even more pronounced for the $2_1^+ \rightarrow 0^+$ transition – its detected angular distribution is isotropic (cf. Table 1) due to the 58.1 (4) ps lifetime of the 2_1^+ state [24,32,39,43]. In our analysis, we were able to determine the angular distribution coefficients for the 1392-keV $(2^-) \rightarrow 2_1^+$ and the 1948-keV $2_2^+ \rightarrow 2_1^+$ transitions (cf. Table 1).

In general, the angular distribution analysis allows for the extraction of the multipole mixing ratios of transitions between excited states. In the case of excited 2^+ levels for which angular distribution coefficients for the transitions to the 2_1^+ state and the ground state are known, this was demonstrated in Ref. [16]. In the present data, however, the transitions to the ground state are either not observed or too weak to allow for extracting the angular distribution coefficients. To overcome this issue, an iterative procedure was applied. The latter is based on fitting the Coulomb excitation yields for a subset of states, namely the 2^+ level of interest, the 2_1^+ and the ground state. The only free parameter in

this subset is the multipole mixing ratio of the transition to the 2_1^+ state. In the first step of the procedure, this transition was assumed to be of pure-dipole character. Low-energy Coulomb excitation on a low-Z target favors one-step E2 transitions resulting in effectively populating the level of interest solely via excitation from the ground state. Resulting matrix elements were used to calculate the statistical tensor for the excited level which, in combination with the experimental angular-distribution coefficients, was used to extract an E2/M1 multipole mixing ratio for the corresponding $2^+ \rightarrow 2_1^+$ transition. This multipole mixing ratio is subsequently used to introduce a quadrupole fraction for the transition to the 2_1^+ state which contributes to the population yield via two-step excitation. This procedure was subsequently applied in an iterative way until the multipole-mixing ratio converged. In this way, a multipole mixing ratio $\delta = 0.26\,(8)$ was determined for the $2_2^+ \rightarrow 2_1^+$ transition (cf. Table 1) indicating its predominant M1 character.

3.2. Lifetime analysis

The DSAM analysis in this work has been performed using a modified version of the computer program `StopSim` [45,46] for the calculation of the excitation and slowing-down of ^{204}Hg nuclei in the Al target and the computer program `APCAD` [45,46] for the calculation of Doppler-broadened γ ray lineshapes and their simultaneous fit to experimental spectra observed under different polar angles of the Gammasphere detectors with respect to the beam axis. The stopping power in Al for ^{204}Hg was extracted from SRIM [47,48]. The γ ray transitions $2_2^+ \rightarrow 2_1^+$, $2_3^+ \rightarrow 2_1^+$ and $3_1^- \rightarrow 4_1^+$ have been considered in this analysis together with several contaminants due to unshifted γ rays. The substantial feeding of the 2_2^+ level by the 3_1^- state was taken into account.

The Doppler-broadened γ ray lineshapes are determined by the lifetimes of the decaying states, the intensities of the γ ray transitions, their angular distributions, the stopping power of the target material for ^{204}Hg and the distributions of ion velocity vectors after the excitation reaction. The latter is calculated by the `StopSim` Monte Carlo simulation code using differential cross sections for CE of the ^{204}Hg nuclei employing the electromagnetic matrix elements obtained from the CE analysis. Two-step excitation of the 2_2^+ and 2_3^+ levels via the 2_1^+ state is taken into account. Since the energy and angle dependencies of the CE cross sections differ for the excitation of the 2_2^+, 2_3^+ and 3_1^- states, different distributions of ion velocity vectors after the reaction are obtained for each of the states. Therefore, simulations have been performed for each of these states separately.

Both the 2_2^+ and 3_1^- states are short-lived, resulting in pronounced Doppler-broadened lineshapes. As a result, the overlapping lineshapes of the very close-lying transitions $2_3^+ \rightarrow 2_1^+$ at $E_0 = 1552.8$ keV and $3_1^- \rightarrow 4_1^+$ at $E_0 = 1547.0$ keV cannot be disentangled in the DSAM analysis. However, their relative intensities and the lifetime of the 2_3^+ state are known from the CE analysis. Therefore, the lineshape of the $2_3^+ \rightarrow 2_1^+$ transition is completely determined and can be derived without free parameters. It was subtracted from the experimental spectra. Subsequently, the lifetimes of the 2_2^+ and 3_1^- states were determined by fits of calculated lineshapes to the data, where, in each case, simulations based on the respective electromagnetic matrix elements were used. The obtained lifetimes are given in Table 1. The data and the fit are displayed in Fig. 3 for three rings of detectors at identical polar angles θ with respect to the beam axis. The quoted uncertainty accounts for the lack of knowledge on the exact stopping power in Al for Hg for which no experimental data exist. This error was determined by varying the SRIM stopping power in the analysis by ±10%. In addition, the uncertainty accounts for the statistics of the data as well as the uncertainty in the 2_3^+ level lifetime, the uncertainty in the $2_3^+ \rightarrow 2_1^+$ intensity, and the uncertainty of the $3_1^- \rightarrow 2_2^+$ feeding intensity which were determined in the CE analysis. The lifetime value for the 2_2^+ level obtained from the DSAM analysis amounts to $84.6^{+14.2}_{-7.4}$ fs, a value which is consistent with the transition rate obtained from the CE analysis.

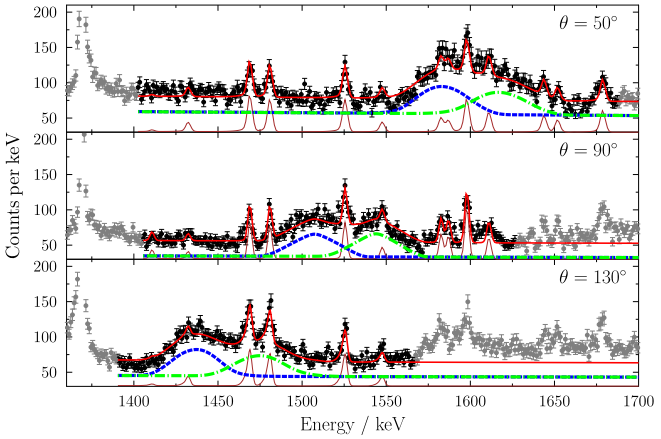

Fig. 3. (Color online.) Experimental DSAM data for three out of 16 polar detector angles and fit of the lineshapes. Only the black data points have been included in the fit. The full fit function is shown in solid red. It is composed of a linear background, the lineshapes of the $2_2^+ \rightarrow 2_1^+$ transition (blue, dashed), the $3_1^- \rightarrow 4_1^+$ transition (green, dashed–dotted) and several contaminant lines (brown). The latter presumably stem from competing reaction channels and are shifted downwards for better visibility. The lineshapes of the $2_2^+ \rightarrow 2_1^+$ and $3_1^- \rightarrow 4_1^+$ transitions are shifted down by 20 counts for better visibility. See the text for details on the lineshape calculation.

4. Discussion

In the present work, we have measured the absolute transition strength $B(M1; 2_2^+ \rightarrow 2_1^+) = 0.200\,(23)\,\mu_N{}^2$ (cf. Table 1). This value is considerably larger than $10^{-2}\,\mu_N{}^2$ typically observed for transitions between FSSs [11] and indicates that the 2_2^+ level at 1948 keV is of isovector nature, which allows us to consider this state at least as a fragment of the one-phonon mixed-symmetry state (MSS) of ^{204}Hg. This conclusion is also supported by the weakly collective ($\sim$ 1 W.u.) E2 decay of the 2_2^+ level to the ground state.

Our result for the one-phonon MSS of ^{204}Hg is similar to the situation reported in the $A \approx 90$ mass region around doubly-magic ^{90}Zr as well as in the $A \approx 60$ mass region around doubly-magic ^{56}Ni, featuring reduced M1 transition matrix elements of single isolated MSSs of the order of $|\langle 2_1^+ \| M1 \| 2_i^+ \rangle| = 1\,\mu_N$ [11]. The $B(M1; 2_2^+ \rightarrow 2_1^+)$ value of ^{204}Hg even holds about one third of the M1 strength of the textbook example $2_{1,ms}^+$ state of ^{94}Mo [8] and is ≈ 1.5 times as large as the $B(M1; 2_2^+ \rightarrow 2_1^+) = 0.126\,(16)\,\mu_N{}^2$ of ^{212}Po [21].

The combination of DSAM lifetime and relative CE intensity measurements allowed to determine E1 strengths of the $3_1^- \rightarrow 2_i^+$ transitions, providing another means for eliminating ambiguities in the identification of the $2_{1,ms}^+$ state [13]. The $B(E1; 3_1^- \rightarrow 2_2^+) = 0.41\,(6)$ mW.u. is ten times larger than the $B(E1; 3_1^- \rightarrow 2_1^+) = 0.041\,(6)$ mW.u. This enhancement in the E1 transition strength reveals the dominant isovector character of the $3_1^- \rightarrow 2_2^+$ transition, while the predominantly isoscalar $3_1^- \rightarrow 2_1^+$ E1 transition is suppressed. This supports further the isovector assignment to the 2_2^+ state. Overall, the E1-decay properties of the 3_1^- state of ^{204}Hg indicate a case that closely resembles those of ^{92}Zr and ^{94}Mo, where similar isovector E1 transition rates were observed [13].

Table 2
QPM calculations of nuclear wave functions.

E_{level} (keV)		J^π	Structure	J_f^π	$\pi\lambda$	$B(\pi\lambda)\downarrow$[a]	
QPM	Exp.					QPM	Exp.
581	436	2_1^+	$69\%[2_1^+]_{RPA} + 14\%[2_1^+ \times 2_1^+]_{RPA}$	0^+	$E2$	8.6	11.96 (9) [39]
1078	1128	4_1^+	$59\%[2_1^+ \times 2_1^+]_{RPA}$	2_1^+	$E2$	16	14.9 (47)
				0^+	$E4$	1.2	5.5 (7) [24]
1751	1948	2_2^+	$79\%[2_2^+]_{RPA}$	2_1^+	$M1$	0.26	0.20 (2)
					$E2$	1.3	1.2 (7)
				0^+	$E2$	1.7	0.28 (2)
2099	1989	2_3^+	$96\%[2_3^+]_{RPA}$	2_1^+	$M1$	0.004	0
					$E2$	0.15	1.55 (38)
				0^+	$E2$	0.13	0.099 (24)
2771	2675	3_1^-	$87\%[3_1^-]_{RPA}$	2_2^+	$E1$	2×10^{-3}	$0.41\,(6) \times 10^{-3}$
				4_1^+	$E1$	0.06×10^{-3}	$0.15\,(2) \times 10^{-3}$
				2_1^+	$E1$	1×10^{-3}	$0.041\,(6) \times 10^{-3}$
				0^+	$E3$	28	20.5 (17)

[a] $B(M1)$ values are given in $\mu_N{}^2$, $B(E\lambda)$ values in W.u. (1 W.u. (E1) = $2.23\,e^2\,fm^2$, 1 W.u. (E2) = $71.3\,e^2\,fm^4$, 1 W.u. (E3) = $2.47 \times 10^3\,e^2\,fm^6$, 1 W.u. (E4) = $9.06 \times 10^4\,e^2\,fm^8$).

The experimental results have been compared to microscopic calculations using the Quasi-particle Phonon Model (QPM) [49]. This approach treats a Hamiltonian of separable form in a microscopic multiphonon basis built of phonons generated in the Quasi-particle Random-Phase Approximation (QRPA). It is, therefore, capable of describing collective modes as well as multiphonon excitations. The parameters of the Woods–Saxon potential are presented in Ref. [50]. The single-particle space includes all shells below the Fermi energy and all bound and quasibound states above the Fermi level. Because of the large model space, the effective charges used are very close to the bare values for protons e_π = 1.05, for neutrons e_ν = 0.05. The spin-gyromagnetic quenching factor used is g_s = 0.8. The strength parameters of the quadrupole–quadrupole and the octupole–octupole potentials are chosen according to the properties of the low-lying 2_1^+ and 3_1^- states, respectively [49,50]. The RPA states are the building blocks of the low-lying multiphonon states. A measure for the quadrupole-collective, symmetric or mixed-symmetric structure of the RPA states is their response to isovector or isoscalar external fields, such as the quantity [51]

$$B(2^+) = \frac{|\langle 2^+ \| \sum_k^{\text{p}} r_k^2\, Y_{2\mu}(\Omega k) - \sum_k^{\text{n}} r_k^2\, Y_{2\mu}(\Omega k) \| g.s. \rangle|^2}{|\langle 2^+ \| \sum_k^{\text{p}} r_k^2\, Y_{2\mu}(\Omega k) + \sum_k^{\text{n}} r_k^2\, Y_{2\mu}(\Omega k) \| g.s. \rangle|^2}.$$

This ratio probes the symmetric (isoscalar) ($B(2^+) < 1$) or mixed-symmetric (isovector) ($B(2^+) > 1$) properties of the 2^+ state under consideration. The value of $B(2^+)$ for the first $\left[2^+\right]_{RPA}$ is 0.016 (symmetric structure) while the same value for the second $\left[2^+\right]_{RPA}$ is 1.06 (mixed-symmetry structure).

The QPM structure of the low-lying states of ^{204}Hg is presented in Table 2, together with a comparison between the experimental and calculated level energies and transition strengths. The structure of the 2_1^+ state is dominated by the $[2_1^+]_{RPA}$ which is predicted to be the one-phonon state of isoscalar nature. The main component in the structure of the 2_2^+ state is the $[2_2^+]_{RPA}$ which is of isovector character. The latter is clearly demonstrated by the large $B(M1; [2_2^+]_{RPA} \to [2_1^+]_{RPA})$ value of $0.48\,\mu_N{}^2$.

The QPM calculations describe the experimental data well. The results are compared to the experimental data in Table 2. The QPM provides good agreement for the excitation energies of the 2_i^+, 3_1^-, and 4_1^+ levels. Furthermore, the calculated $B(E2; 2_1^+ \to 0^+)$ = 8.6 W.u. is quite close to the experimental value of 11.96 (9) W.u. [39]. In addition, there is a good agreement between the calculated and the experimental $B(E3; 3_1^- \to 0^+)$ values (cf. Table 2) as both of them are close to the adopted literature value of 23 (2) W.u. [39]. Moreover, an agreement of the same quality between the present experimental result, the QPM calculations and the previously known value of 17.0 (13) W.u. [31,32,39] is achieved for the $B(E2; 4_1^+ \to 2_1^+)$ transition strength (cf. Table 2). The overall agreement between the QPM results on level energies, E2 and E3 transition strengths and the experimental data demonstrates the predictive power of the QPM, even in mass regions where the model is applied for the first time for the description of MSSs. Concerning the E1 transitions the calculated values are small but differ from the experimental ones. This may be due to the fact that the QPM results strongly depend on the large amount of components contributing weakly to the structure of the 3_1^- and 2_1^+ states. The first 3^- and 2^+ states are collective and it is not possible to select the main components contributing to E1 transitions.

The QPM predicts negligible M1 transition strengths for almost all $2_i^+ \to 2_1^+$ transitions. The sole exception is the $2_2^+ \to 2_1^+$ transition for which $B(M1) = 0.26\,\mu_N{}^2$ is calculated. This result is close to the experimental value of $0.20\,(2)\,\mu_N{}^2$. Moreover, the QPM predicts that the 2_2^+ state decays by a weak E2 transition to the ground state and that the 3_1^- level decays by a relatively enhanced E1 transition (with respect to the $3_1^- \to 2_1^+$ one) to the 2_2^+ state, in qualitative agreement with expectation for a E1 transition connecting isoscalar and isovector states.

The overall good agreement between the QPM calculations and the experimental results for the properties of the 2_2^+ state of ^{204}Hg, combined with the predominant isovector character of the second $[2^+]_{\text{RPA}}$ solution confirms the conclusion that the 2_2^+ state of ^{204}Hg is the main fragment of the $2_{1,ms}^+$ state. Apparently, the low-lying $2_i^+ \to 2_1^+$ isovector M1 strength is concentrated in a single state.

5. Summary

A combination of projectile Coulomb excitation and DSAM measurements was carried out to identify the $2_{1,ms}^+$ state of ^{204}Hg for the first time. The lifetime and transition strengths of this non-yrast 2^+ level were determined. The measured absolute M1 transition strength enables the interpretation of the 2_2^+ state of ^{204}Hg as the main fragment of the $2_{1,ms}^+$ state. This suggestion is strongly supported by the performed QPM calculations. It indicates that, in ^{204}Hg, the low-lying M1 transition strength is concentrated in a single isolated state.

Acknowledgements

G.R. acknowledges the support from the Alexander von Humboldt foundation. This material is based upon work supported by

the U.S. Department of Energy, Office of Science, Office of Nuclear Physics, under contract number DE-AC02-06CH11357. This research used resources of ANL's ATLAS facility, which is a DOE Office of Science User Facility. This work was supported by the German-Bulgarian exchange program under grants DAAD No. PPP57082997 and BgNSF No. DNTS/01/05/2014 and DN08/23, and by the BMBF under grant Nos. 05P12RDCIB, 05P15RDFN1 and 05P15RDCIA.

References

[1] C. Kremer, et al., Phys. Rev. Lett. 117 (2016) 172503.
[2] T. Togashi, et al., Phys. Rev. Lett. 117 (2016) 172502.
[3] A. Arima, T. Ohtsuka, F. Iachello, I. Talmi, Phys. Lett. B 66 (1977) 205.
[4] F. Iachello, Phys. Rev. Lett. 53 (1984) 1427.
[5] F. Iachello, A. Arima, The Interacting Boson Model, Cambridge University Press, Cambridge, 1987.
[6] T. Ahn, et al., Phys. Lett. B 679 (2009) 19.
[7] W.D. Hamilton, A. Irbäck, J.P. Elliott, Phys. Rev. Lett. 53 (1984) 2469.
[8] N. Pietralla, et al., Phys. Rev. Lett. 83 (1999) 1303.
[9] N. Pietralla, et al., Phys. Rev. Lett. 84 (2000) 3775.
[10] U. Kneissl, N. Pietralla, A. Zilges, J. Phys. G, Nucl. Part. Phys. 32 (2006) R217.
[11] N. Pietralla, P. von Brentano, A. Lisetskiy, Prog. Part. Nucl. Phys. 60 (2008) 225.
[12] N.A. Smirnova, et al., Nucl. Phys. A 678 (2000) 235.
[13] N. Pietralla, et al., Phys. Rev. C 68 (2003) 031305.
[14] N. Pietralla, et al., Phys. Rev. C 64 (2001) 031301.
[15] V. Werner, et al., Phys. Lett. B 550 (2002) 140.
[16] G. Rainovski, et al., Phys. Rev. Lett. 96 (2006) 122501.
[17] L. Coquard, et al., Phys. Rev. C 82 (2010) 024317.
[18] K.A. Gladnishki, et al., Phys. Rev. C 82 (2010) 037302.
[19] M. Danchev, et al., Phys. Rev. C 84 (2011) 061306.
[20] T. Ahn, et al., Phys. Rev. C 86 (2012) 014303.
[21] D. Kocheva, et al., Phys. Rev. C 93 (2016) 011303.
[22] I.-Y. Lee, Nucl. Phys. A 520 (1990) 641c.
[23] D.A. Craig, H.W. Taylor, J. Phys. G, Nucl. Part. Phys. 10 (1984) 1133.
[24] A.J.C. Burghardt, Ph.D. thesis, University of Amsterdam, 1989.
[25] R. Gatenby, E. Kleppinger, S. Yates, Nucl. Phys. A 492 (1989) 45.
[26] A. Hogenbirk, H. Blok, M. Harakeh, Nucl. Phys. A 524 (1991) 251.
[27] P. Schuler, et al., Z. Phys. A 317 (1984) 313.
[28] R.A. Moyer, Phys. Rev. C 5 (1972) 1678.
[29] A.M. Baxter, et al., Nucl. Phys. A 369 (1981) 25.
[30] A.R. Poletti, et al., Nucl. Phys. A 580 (1994) 64.
[31] Y.K. Agarwal, et al., Z. Phys. A 320 (1985) 295.
[32] M.T. Esat, et al., Nucl. Phys. A 362 (1981) 227.
[33] C.S. Lim, W.N. Catford, R.H. Spear, Nucl. Phys. A 522 (1991) 635.
[34] E.N.M. Quint, et al., Phys. Rev. Lett. 58 (1987) 1088.
[35] H. Backe, et al., Nucl. Phys. A 189 (1972) 472.
[36] T. Dubler, et al., Nucl. Phys. A 294 (1978) 397.
[37] P. Grabmayr, et al., Nucl. Phys. A 494 (1989) 244.
[38] F.D. Becchetti, et al., Phys. Rev. C 19 (1979) 1775.
[39] C. Chiara, F. Kondev, Nucl. Data Sheets 111 (2010) 141.
[40] T. Kibédi, et al., Nucl. Instrum. Methods Phys. Res., Sect. A 589 (2008) 202.
[41] K. Alder, A. Winther, Electromagnetic excitation: Theory of Coulomb excitation with heavy ions, North-Holland Publishing Company, Amsterdam–Oxford, 1975.
[42] H. Ower, Ph.D. thesis, Johann Wolfgang Goethe-Universität Frankfurt am Main, 1980.
[43] A. Bockisch, K. Bharuth-Ram, A.M. Kleinfeld, K.P. Lieb, Z. Phys. A 291 (1979) 245.
[44] A.E. Stuchbery, P.F. Mantica, A.N. Wilson, Phys. Rev. C 71 (2005) 047302.
[45] C. Stahl, Ph.D. thesis, Technische Universität Darmstadt, July 2015.
[46] C. Stahl, et al., Comput. Phys. Commun. 214 (2017) 174.
[47] J.F. Ziegler, M. Ziegler, J. Biersack, Nucl. Instrum. Methods Phys. Res., Sect. B, Beam Interact. Mater. Atoms 265 (2010) 1818.
[48] http://www.srim.org.
[49] N. Lo Iudice, et al., J. Phys. G, Nucl. Part. Phys. 39 (2012) 043101.
[50] S. Galès, C. Stoyanov, A. Vdovin, Phys. Rep. 166 (1988) 125.
[51] R. Nikolaeva, C. Stoyanov, A.I. Vdovin, Europhys. Lett. 8 (1989) 117.